# Sigma-Point Kalman Filtering for Spacecraft Attitude and Rate Estimation using Magnetometer Measurements

**MOHAMMAD ABDELRAHMAN**
**SANG-YOUNG PARK**
Yonsei University

**A generalized algorithm for spacecraft three-axis attitude and rate estimation is presented. The filter concept presented here is quite general and applicable to a wide range of sensor systems. The structure of the filter is built using spacecraft nonlinear dynamics in the presence of momentum exchange devices. Then quaternion kinematics are augmented with spacecraft dynamics to represent the filter process dynamics. Magnetometer measurements and their corresponding time derivatives are utilized to represent the filter measurement model. The filter is designed to suit spacecraft in low-Earth orbits, so the aerodynamic drag in addition to spacecraft magnetic residuals are included as disturbance torques to the process dynamics. To test the filter EgyptSat-1 is used as a real test case where a magnetometer and fiber-optic gyros are used for attitude and rate determination. A Monte-Carlo simulation is then applied to study the performance of the proposed filter with initial attitude and angular velocity sampled from a uniform distribution, each axis respectively. The filter shows the capability of estimating the attitude within 5 deg and rate on the order of 0.03 deg/s in each axis.**

Manuscript received February 29, 2008; revised May 19, 2009; released for publication February 5, 2010.

IEEE Log No. T-AES/47/2/940853.

Refereeing of this contribution was handled by P. Willett.

This work was supported by the Korea Science and Engineering Foundation (KOSEF) through the National Research Laboratory Program funded by the Ministry of Science and Technology (M10600000282-06J0000-28210).

Authors' address: Astrodynamics and Control Laboratory, Department of Astronomy, Yonsei University, 134 Shinchon-dong, Seoul, 120-749, South Korea, E-mail: (spark624@yonsei.ac.kr).



## I. INTRODUCTION

The presented work is a continuation of previous efforts by the authors and others that have addressed the problem of magnetometer-based three-axis attitude and rate determination. The majority of the literature that has dealt with the combined attitude and rate estimation is based on using at least two vector measurements or one reference sensor in the presence of rate gyros. Hill and McCusker [1] developed a simple real-time algorithm using horizon sensor and magnetometer data for a full-attitude solution in Euler angles; the body rates are obtained by differentiating the angles with appropriate filtering to reduce the noise. Azor et al. [2] and Bar-Itzhack et al. [3] presented two different approaches for attitude rate estimation with a prior attitude knowledge derived from two vector measurements or a star sensor data. The first approach is based on the time derivatives of vector measurements expressed in reference and body coordinates. Because of the induced high-frequency noise resulting from measurement differentiation, some filtering is incorporated to suppress that noise. The filter can be a passive low-pass filter or an active filter like the extended Kalman filter (EKF), extended interlaced Kalman filter, state-dependent algebraic Riccati equation (SDARE) filter, or pseudo linear Kalman (PSELIKA) filter. The second approach, which is called the estimation approach, avoids differentiation by applying an estimator directly to the raw measurements. The kinematics equation, which relates the attitude parameters to the angular rate, is used as a part of the estimator. During anomalous conditions like eclipse and/or measurement vectors coalignment, the attitude cannot be determined; also during high-rate maneuvers the quaternion measurements cannot be provided when using a star sensor/tracker. The approach of Challa et al. [4] estimates the three-axis attitude and rate using only magnetometer data. The estimation system uses the EKF that includes Euler dynamics for rate propagation, and it achieves accuracies on the order of several degrees. Initialization is sometimes handled by a deterministic batch algorithm. The authors report that their filter convergences without a good prior attitude or rate knowledge, but they give no guarantee that their initialization techniques will work reliably in all circumstances. Crassidis and Markley [5] derived a real-time predictive filter for spacecraft attitude estimation without utilizing gyro measurements. The filtering algorithm is based on a predictive tracking scheme introduced by Lu [6], which is developed basically to solve control problems. The formulation is derived to suit the utilization of reference sensors. This approach determines the optimal spacecraft attitude in real time by minimizing a quadratic cost function consisting of a measurement residual term and a model error term. Although the algorithm

is shown to be capable of estimating the attitude and rate during normal modes when more than one vector measurement is used and when only one sensor measurement is available, the authors do not guarantee the stability or the observability of the filter. Also the filter has not been tested for different initial conditions or even compared with the traditional EKF algorithm. Humphreys et al. [7] developed a magnetometer-based EKF system for attitude and rate estimation for a gravity-gradient stabilized spacecraft. It uses Euler's equation to propagate rates, but it requires a reasonable initialization in order to converge. Also Psiaki [8] introduced a self-initializing attitude determination filter to estimate the three-axis attitude and rate from magnetometer data only. It uses a new attitude parameterization that is based on perturbations of the minimum quaternion that aligns the magnetic field in reference coordinates with the field in spacecraft coordinates. The filter model includes Euler dynamics and attitude kinematics, and its least-squares cost function penalizes magnetometer measurement errors and torque process noise. The filtering algorithm includes an initialization procedure, which automatically finds a reasonable initial estimate that causes the EKF to converge. The validity of the implicit dynamics (quaternion/Euler) models depends on having a short magnetometer sample interval; otherwise the trapezoidal integration approximation used will break down. Moreover the spacecraft might violate the assumption of the new attitude parameters which assumes its rotation to be less than 180 deg between samples.

The main objectives of the current paper are to develop a generalized filter for attitude and rate estimation which should be independent of the type of the spacecraft (spinning, gravity-gradient, or momentum biased). It should be suited for three-axis stabilized Earth pointing spacecraft with a minimum equipment list (MEL). Thus the attitude and rate estimation algorithm is required to utilize mainly one low-cost reference sensor but with the ability to be modular for any additional sensor assembly (reference/inertial or reference/reference). Also the filter should accommodate large initial errors and avoid any linearization approximations regarding the attitude dynamics, attitude parameters, and uncertainty transformation, without any additional computing complexity such as Jacobians. In addition to achieving the previous objectives, the filter works as a main attitude/rate estimation algorithm for the test case at hand and not as a contingency algorithm in the case of sensor failure, which is the essential focus of much former research based on using single-sensor measurements. It estimates the attitude and rates during satellite detumbling and standby modes where the magnetometer measurements alone can fulfill the mission attitude and rate accuracy requirements for these two modes. In these instances the estimated attitude and rates are used for driving the controller of the satellite; the control torque levels are compared with these attitudes and rate estimates, which result when using a magnetometer/gyro assembly for attitude and rate estimation. Magnetometer measurements are used throughout this paper only due to the hardware configuration of the test case, but any other single vector measurement such as the Sun vector can be used.

The paper is organized first to review the concept of sigma-point Kalman filtering (SPKF) with a brief discussion about its advantages over the well-known Kalman filtering technique. Then the filter architecture is presented through the derivation of the process and observation models. Finally the performance and stability of the proposed filter is tested and compared with the EKF using simulated three-axis magnetometer data.

## II. THE SIGMA-POINT KALMAN FILTERING

The SPKFs handle the approximation problems of the EKF. This is achieved through a fundamentally different approach for calculating the posterior first- and second-order statistics of a random variable that undergoes a nonlinear transformation. The state distribution is represented by a Gaussian random variable (GRV), but it is specified using a minimal set of deterministically chosen weighted sample points. These samples, called sigma-points, completely capture the true mean and covariance of the prior random variable, and when propagated through the true nonlinear system, capture the posterior mean and covariance accurately to the second order for any nonlinearity. The basic sigma-point approach (SPA) can be described as follows [9–11].

1) A set of weighted samples (sigma-points) are deterministically calculated using the mean and square-root decomposition of the covariance matrix of the prior random variable. As a minimal requirement the sigma-point set must completely capture the first- and second-order moments of the prior random variable. Higher order moments can be captured if so desired, at the cost of using more sigma-points.

2) The sigma-points are propagated through the true nonlinear function using functional evaluations alone, i.e., no analytical derivatives are used in order to generate a posterior sigma-point set.

3) The posterior statistics are calculated (approximated) using tractable functions of the propagated sigma-points and weights. Typically these take on the form of simple weighted sample mean and covariance calculations of the posterior sigma-points.

### A. The Unscented Kalman Filter

From the family of SPKF the unscented Kalman filter (UKF) derives the location of the sigma-points as well as their corresponding weights according to the following rationale [12]: The sigma-points should

be chosen so that they capture the most important statistical properties of the prior random variable $\mathbf{x}$ with a probability density $p(\mathbf{x})$. This is achieved by choosing the points according to a constraint equation of the form $\zeta(\langle\chi, W\rangle, r, p(\mathbf{x})) = 0$, where $\langle\chi, W\rangle$ is the set of all sigma-points $\chi_i$ and weights $W_i$ for $i = 1, \ldots r$.

It is possible to satisfy such a constraint condition and still have some degree of freedom in the choice of the point locations by minimizing a further penalty or cost function of the form $c(\langle\chi, W\rangle, r, p(\mathbf{x}))$. The purpose of this cost function is to incorporate statistical features of $\mathbf{x}$ which are desirable but do not necessarily have to be met. In other words the sigma-points are given by the solution to the following optimization problem:

$$\begin{aligned} &\min_{\langle\chi, W\rangle} c(\langle\chi, W\rangle, r, p(\mathbf{x})) \\ &\text{subject to} \quad \zeta(\langle\chi, W\rangle, r, p(\mathbf{x})) = 0. \end{aligned} \tag{1}$$

The necessary statistical information captured by the UKF is the first- and second-order moments of $p(\mathbf{x})$. The number of sigma-points needed to do this is $r = 2L + 1$, where $L$ is the dimension of $\mathbf{x}$ [11] and [12].

In order to illustrate the UKF algorithm for state estimation, consider that the state vector $\mathbf{x}$ is given at step $k-1$ with error covariance matrix $\mathbf{P}$; then a collection of sigma-points is computed and stored in the columns of the $L \times (2L + 1)$ sigma-point matrix $\chi_{k-1}$. The columns of $\chi_{k-1}$ are computed by

$$\begin{aligned} (\chi_{k-1})_0 &= \hat{\mathbf{x}}_{k-1} \\ (\chi_{k-1})_i &= \hat{\mathbf{x}}_{k-1} + \left(\sqrt{(L+\lambda)\mathbf{P}_{k-1}}\right)_i, \qquad i = 1 \ldots L \\ (\chi_{k-1})_i &= \hat{\mathbf{x}}_{k-1} - \left(\sqrt{(L+\lambda)\mathbf{P}_{k-1}}\right)_{i-L}, \qquad i = L+1 \ldots 2L \end{aligned} \tag{2}$$

where $(\sqrt{(L+\lambda)\mathbf{P}_{k-1}})_i$ is the $i$th column of the matrix square root, and $\lambda$ is defined by

$$\lambda = \alpha^2(L + \kappa) - L \tag{3}$$

where $\alpha$ is a scaling parameter which determines the spread of the sigma-points, and $\kappa$ is a secondary scaling parameter. The matrix $(\sqrt{(L+\lambda)\mathbf{P}_{k-1}})_i$ is assumed to be symmetric and positive definite, which allows to find the square root using a Cholesky decomposition.

Once $\chi_{k-1}$ is computed the prediction step is performed by propagating each column of $\chi_{k-1}$ through time by $\Delta t$ using

$$(\chi_k)_i = f((\chi_{k-1})_i), \qquad i = 0 \ldots 2L \tag{4}$$

where $f$ is a set of differential equations describing the process dynamics. With $(\chi_k)_i$ calculated, the a priori state estimated is

$$\hat{\mathbf{x}}_k^- = \sum_{i=0}^{2L} W_i^{(m)} (\chi_k)_i \tag{5}$$

where $W_i^{(m)}$ are weights defined by

$$\begin{aligned} W_0^{(m)} &= \frac{\lambda}{(L+\lambda)} \\ W_i^{(m)} &= \frac{1}{2(L+\lambda)}, \qquad i = 1 \ldots 2L. \end{aligned} \tag{6}$$

The last part of the predication is accomplished with the calculation of the prior error covariance

$$\mathbf{P}_k^- = \sum_{i=0}^{2L} W_i^{(c)} [(\chi_k)_i - \hat{\mathbf{x}}_k^-][(\chi_k)_i - \hat{\mathbf{x}}_k^-]^T + \mathbf{Q}_k \tag{7}$$

where $\mathbf{Q}_k$ is the discrete process error covariance matrix, and the weights are defined by

$$\begin{aligned} W_0^{(c)} &= \frac{\lambda}{(L+\lambda)} + (1 - \alpha^2 + \beta) \\ W_i^{(c)} &= \frac{1}{2(L+\lambda)}, \qquad i = 1 \ldots 2L. \end{aligned} \tag{8}$$

Note that $\beta$ is a parameter used to incorporate any prior knowledge about the distribution of $\mathbf{x}$.

To compute the correction step the columns of $\chi_k$ must be transformed through the measurement function. Therefore let

$$(\mathbf{Z}_k)_i = h((\chi_k)_i), \qquad i = 0 \ldots 2L \tag{9}$$

$$\hat{\mathbf{z}}_k^- = \sum_{i=0}^{2L} W_i^{(m)} (\mathbf{Z}_k)_i \tag{10}$$

where $h$ is the measurement equation. With the transformed state vector $\hat{\mathbf{z}}_k^-$, the posterior state estimate is computed

$$\hat{\mathbf{x}}_k = \hat{\mathbf{x}}_k^- + \mathbf{K}_k(\mathbf{z}_k - \hat{\mathbf{z}}_k^-). \tag{11}$$

The true measurement is represented by $\mathbf{z}_k$, while the Kalman gain $\mathbf{K}_k$ formulation in the UKF is defined by

$$\mathbf{K}_k = \mathbf{P}_{\hat{x}_k \hat{z}_k} \mathbf{P}_{\hat{z}_k \hat{z}_k}^{-1} \tag{12}$$

where

$$\mathbf{P}_{\hat{z}_k \hat{z}_k} = \sum_{i=0}^{2L} W_i^{(c)} [(\mathbf{Z}_k)_i - \hat{\mathbf{z}}_k^-][(\mathbf{Z}_k)_i - \hat{\mathbf{z}}_k^-]^T + \mathbf{R} \tag{13}$$

$$\mathbf{P}_{\hat{x}_k \hat{z}_k} = \sum_{i=0}^{2L} W_i^{(c)} [(\chi_k)_i - \hat{\mathbf{x}}_k^-][(\mathbf{Z}_k)_i - \hat{\mathbf{z}}_k^-]^T. \tag{14}$$

As with the EKF the matrix $\mathbf{R}$ is the measurement noise covariance matrix. Finally the last calculation in the correction step is to compute the posteriori estimate of the error covariance given by

$$\mathbf{P}_k = \mathbf{P}_k^- - \mathbf{K}_k \mathbf{P}_{\hat{z}_k \hat{z}_k} \mathbf{K}_k^T. \tag{15}$$

Note that no explicit calculations of Jacobians or Hessians are necessary to implement this algorithm. Furthermore the overall number of computations is small enough to be used in real-time applications.

## III. FILTER ARCHITECTURE

In this section the filter process and observation models are presented through the spacecraft attitude dynamics and kinematics with the candidate attitude determination hardware.

### A. Spacecraft Attitude Dynamics

The generalized dynamic model is represented by Euler's equations in the presence of momentum exchange devices and is given by

$$\mathbf{I}\dot{\boldsymbol{\omega}} + \dot{\mathbf{h}} + \boldsymbol{\omega} \times (\mathbf{I}\boldsymbol{\omega} + \mathbf{h}) = \mathbf{T}. \tag{16}$$

Rearranging, we have

$$\dot{\boldsymbol{\omega}} = -\mathbf{I}^{-1}[\boldsymbol{\omega} \times (\mathbf{I}\boldsymbol{\omega} + \mathbf{h})] + \mathbf{I}^{-1}(\mathbf{T} - \dot{\mathbf{h}}). \tag{17}$$

The angular velocity vector $\boldsymbol{\omega}$ represents the rotation of body coordinates $b$ with respect to inertial coordinates $i$. The matrix $\mathbf{I}$ is the spacecraft mass moment of inertia, $\mathbf{h}$ is the angular momentum vector of the momentum/reaction wheels, and $\mathbf{T}$ is the total torque vector exerted on the spacecraft which includes the following:

*Gravity gradient torque*:

$$\mathbf{T}_{gg} = \frac{3\mu}{|\mathbf{R}|^3}[\hat{\mathbf{R}} \times (\mathbf{I}\hat{\mathbf{R}})] \tag{18}$$

where $\mathbf{R}$ is the position vector, and $\mu$ is the Earth's gravitational constant.

*Aerodynamic torque*:

$$\mathbf{T}_{\text{aero}} = \tfrac{1}{2}C_d\rho|\mathbf{V}_{\text{rel}}|^2\sum_{i=1}^{n}(\hat{\mathbf{N}}_i \cdot \hat{\mathbf{V}}_{\text{rel}})(\hat{\mathbf{V}}_{\text{rel}} \times \mathbf{r}_i)A_i. \tag{19}$$

The summation is taken over $n$ surfaces of the spacecraft with area $A_i$ and unit outward normal vector $\hat{\mathbf{N}}_i$. The parameter $C_d$ is the drag coefficient, and $\rho$ is the atmospheric density. The velocity vector relative to the rotating atmosphere $\mathbf{V}_{\text{rel}}$ is

$$\mathbf{V}_{\text{rel}} = \mathbf{V} - \boldsymbol{\omega}_{\oplus} \times \mathbf{R} \tag{20}$$

where $\boldsymbol{\omega}_{\oplus}$ is the Earth's rotational velocity, and $\mathbf{V}$ is the spacecraft velocity.

*Magnetic disturbance torque*:

$$\mathbf{T}_m = \mathbf{m} \times \mathbf{B}. \tag{21}$$

The spacecraft dipole moment is the vector $\mathbf{m}$ while $\mathbf{B}$ is the Earth's magnetic field.

*Control torque*: The form of the control torque is quite arbitrary and depends on the control strategy used for the fulfillment of the mission requirements. For the test case presented in this paper a proportional plus derivative (PD) controller is used

$$\mathbf{T}_c = -\mathbf{K}_p q_{4e}^{br}\mathbf{q}_{13e}^{br} - \mathbf{K}_v\boldsymbol{\omega}^{br}. \tag{22}$$

The diagonal matrices $\mathbf{K}_p$ and $\mathbf{K}_v$ are the position and velocity control gains, respectively. The angular velocity vector $\boldsymbol{\omega}^{br}$ used in the control law is the rotation of body coordinates $b$ with respect to reference (orbit) coordinates $r$. The attitude error is represented by the error quaternion $\mathbf{q}_e^{br}$, which is described in the next subsection.

Finally the total torque is

$$\mathbf{T} = \mathbf{T}_{gg} + \mathbf{T}_{\text{aero}} + \mathbf{T}_m + \mathbf{T}_c. \tag{23}$$

Note all vectors in the previous equations are derived in the spacecraft body frame.

### B. Quaternion Kinematics

The spacecraft attitude is represented through the quaternion, defined by

$$\mathbf{q} \equiv \begin{bmatrix}\mathbf{q}_{13}\\ q_4\end{bmatrix} \tag{24}$$

where

$$\mathbf{q}_{13} \equiv \begin{bmatrix}q_1\\ q_2\\ q_3\end{bmatrix} = \hat{\mathbf{n}}\sin(\phi/2) \tag{25a}$$

$$q_4 = \cos(\phi/2) \tag{25b}$$

$\hat{\mathbf{n}}$ is a unit vector corresponding to the axis of rotation, and $\phi$ is the angle of rotation. The quaternion kinematics are derived through the spacecraft's angular velocity as follows:

$$\dot{\mathbf{q}} = \tfrac{1}{2}\boldsymbol{\Omega}(\boldsymbol{\omega})\mathbf{q} = \tfrac{1}{2}\boldsymbol{\Xi}(\mathbf{q})\boldsymbol{\omega} \tag{26}$$

where $\boldsymbol{\Omega}(\boldsymbol{\omega})$ and $\boldsymbol{\Xi}(\mathbf{q})$ are defined as

$$\boldsymbol{\Omega}(\boldsymbol{\omega}) = \begin{bmatrix}-[\boldsymbol{\omega}\times] & \vdots & \boldsymbol{\omega}\\ \cdots & \vdots & \cdots\\ -\boldsymbol{\omega}^T & \vdots & \mathbf{0}\end{bmatrix} \tag{27a}$$

$$\boldsymbol{\Xi}(\mathbf{q}) = \begin{bmatrix}q_4\mathbf{I}_{3\times 3} + [\mathbf{q}_{13}\times]\\ \cdots\\ -\mathbf{q}_{13}^T\end{bmatrix}. \tag{27b}$$

Here $\mathbf{I}_{3\times 3}$ is a unit matrix, and the $3 \times 3$-dimensional matrices $[\boldsymbol{\omega}\times]$ and $[\mathbf{q}_{13}\times]$ are defined as skew-symmetric matrices

$$[\mathbf{u}\times] = \begin{bmatrix}0 & -u_3 & u_2\\ u_3 & 0 & -u_1\\ -u_2 & u_1 & 0\end{bmatrix}. \tag{28}$$

The quaternion four elements satisfy the following normalization constraint

$$\mathbf{q}^T\mathbf{q} = \mathbf{q}_{13}^T\mathbf{q}_{13} + q_4^2 = 1. \tag{29}$$

Recall the control law in (22), the error quaternion $\mathbf{q}_e^{br}$ is defined as

$$\mathbf{q}_e^{br} = \mathbf{q}_S^{br} \otimes \mathbf{q}_T^{-1} = \begin{bmatrix}q_{4T}\mathbf{q}_{13S}^{br} - q_{4S}^{br}\mathbf{q}_{13T} + \mathbf{q}_{13S}^{br} \times \mathbf{q}_{13T}\\ \cdots\cdots\cdots\cdots\cdots\\ q_{4S}^{br}q_{4T} + \mathbf{q}_{13S}^{br} \cdot \mathbf{q}_{13T}\end{bmatrix} \tag{30}$$

where $\mathbf{q}_S^{br}$ is the spacecraft quaternion describing the attitude with respect to the reference frame, and $\mathbf{q}_T$ is the target (desired) quaternion.

### C. Process Model

The spacecraft dynamic model is augmented with the quaternion kinematics in (17) and (26), to build up the system process model. The availability of the telemetry data during the commissioning phase of the test case, especially through the imaging mode, is utilized to reconstruct the attitude dynamics model. During the imaging mode full-state measurements are provided via a star sensor and fiber-optic gyros in addition to the navigation information through a GPS receiver. The enhancement of the disturbance torques models/parameters is one of the major aspects in the attitude model reconstruction. So due to the interference between the magnetometer and torque rods which are used as main actuators during detumbling and standby modes, the satellite dipole moment is added to the state vector. Also the aerodynamic drag coefficient is included in the state vector for more filter robustness. Moreover recall that the disturbance torque models in (19) and (21), in the presence of attitude information and navigation data besides the magnetometer measurements during the attitude model reconstruction process, have been used for modeling the spacecraft dipole moment and the aerodynamic drag coefficient as an average/nominal value with additive uncertainties that have been tuned for better attitude model reconstruction.

The filter state vector $\mathbf{x}$ is eleven-dimensional, defined as

$$\mathbf{x} = [\boldsymbol{\omega}^T, \mathbf{q}^T, \mathbf{m}^T, C_d]. \tag{31}$$

Then the filter process can be formulated as

$$\begin{bmatrix} \dot{\boldsymbol{\omega}} \\ \cdots \\ \dot{\mathbf{q}} \\ \cdots \\ \dot{\mathbf{m}} \\ \cdots \\ \dot{C}_d \end{bmatrix} = \begin{bmatrix} -\mathbf{I}^{-1}[\boldsymbol{\omega} \times (\mathbf{I}\boldsymbol{\omega} + \mathbf{h})] + \mathbf{I}^{-1}(\mathbf{T} - \dot{\mathbf{h}}) \\ \cdots\cdots\cdots\cdots\cdots \\ \tfrac{1}{2}\boldsymbol{\Xi}(\mathbf{q})\boldsymbol{\omega} \\ \cdots\cdots\cdots\cdots\cdots \\ \mathbf{0}_{3\times 1} \\ \cdots\cdots\cdots\cdots\cdots \\ 0 \end{bmatrix} + \begin{bmatrix} \boldsymbol{\nu}_\omega \\ \cdots \\ \mathbf{0}_{4\times 1} \\ \cdots \\ \boldsymbol{\nu}_m \\ \cdots \\ \nu_c \end{bmatrix} \tag{32}$$

$$\dot{\mathbf{x}} = f(\mathbf{x}, t) + \boldsymbol{\nu}_x(t).$$

The process noise is added through the vector $\nu_x$, which consists of four subvectors. The first one represents the torque noise (ripples) resulting from control actuators such as magnetorquers and reaction wheels, the third and fourth vectors are the time variations of the spacecraft dipole and drag coefficient, while the second vector is a zero vector.

### D. Observation Model and Attitude Determination Hardware

The proposed algorithm is oriented to the utilization of only one reference sensor, so the default observation equation is that which relates the sensor output to a reference model through a certain transformation. Therefore the measurement model is assumed to be of the form given by

$$\mathbf{B}_b = \mathbf{A}\mathbf{B}_i \tag{33}$$

where $\mathbf{B}_i$ is a vector of some reference such as the position vector to the Sun, to a star, or the Earth's magnetic field vector in a reference coordinate system; and $\mathbf{B}_b$ is the corresponding measured vector (from Sun, star, Earth sensor or a magnetometer) in the spacecraft body frame; and the transformation matrix $\mathbf{A}$ is given by

$$\mathbf{A} = (q_4^2 - \mathbf{q}_{13}^T\mathbf{q}_{13})\mathbf{I}_{3\times 3} + 2\mathbf{q}_{13}\mathbf{q}_{13}^T - 2q_4[\mathbf{q}_{13}\times]. \tag{34}$$

Equation (33) directly relates the measurements to the attitude, but it gives no additional information about the angular rate. Another set of measurements is added using vector dynamics to calculate the time derivatives of the measurements

$$\mathbf{A}\dot{\mathbf{B}}_i = \dot{\mathbf{B}}_b + \boldsymbol{\omega} \times \mathbf{B}_b. \tag{35}$$

Rearranging, we have

$$\dot{\mathbf{B}}_b = \mathbf{A}\dot{\mathbf{B}}_i - \boldsymbol{\omega} \times [\mathbf{A}\mathbf{B}_i]. \tag{36}$$

Augmenting (33) with (36), the nonlinear observation model is formulated:

$$\begin{bmatrix} \mathbf{B}_b \\ \cdots \\ \dot{\mathbf{B}}_b \end{bmatrix} = \begin{bmatrix} \mathbf{A}\mathbf{B}_i \\ \cdots\cdots \\ \mathbf{A}\dot{\mathbf{B}}_i - \boldsymbol{\omega} \times [\mathbf{A}\mathbf{B}_i] \end{bmatrix} + \begin{bmatrix} \boldsymbol{\nu}_B \\ \cdots \\ \boldsymbol{\nu}_{\dot{B}} \end{bmatrix}$$
$$\mathbf{z} = h(\mathbf{x}, t) + \boldsymbol{\nu}_z(t) \tag{37}$$

where $\nu_z$ is the observation noise vector including two subvectors $\boldsymbol{\nu}_B$ and $\boldsymbol{\nu}_{\dot{B}}$ for the measured vector and its time-derivative noises, respectively. All the noise vectors added in the process and observation models are zero-mean white noise.

The control loop of the attitude determination and control subsystem (ADCS) usually has an overall sampling time larger than the sampling time of the magnetometer which is considered a fast sensor. So during one sampling interval, several magnetometer readings can be obtained. Then the time derivatives of the magnetic field measurements are computed in a semi-analytical method via differentiating the

polynomials resulting from a cubic spline fit of the measurement data during each sampling interval. A reasonable number of readings during the sampling interval is utilized since using a low number results in poor presentation of the magnetic field, and a high number results in very noisy derivatives. This method is considered a mapping of the unprocessed measurements sets along the sampling interval to create another set of new measurements (derivatives). Hence an assumption of having an additional separate virtual sensor for magnetic field rates can be applied.

From the above observation model it can obviously be seen that the added set of measurements is expected to guarantee the system local observability since every state variable $(\boldsymbol{\omega}, \mathbf{q})$ of the system affects the outputs in (37).

## IV. FILTER PERFORMANCE AND TESTING

The reasons for developing the presented filter are the lessons experienced from launching EgyptSat-1 during the commissioning phase. EgyptSat-1 is the first Egyptian remote sensing satellite launched on April 17, 2007. The ADCS was supposed to provide three-axis attitude and rate information during standby (nominal/hibernation) mode, not worse than 5 deg and 0.03 deg/s, respectively. The hardware dedicated to achieving these requirements is a three-axis magnetometer with only an attitude control based on using magnetorquers in a momentum bias system.

The ADCS strategy succeed in capturing the satellite after launching, but it failed to fulfill the standby requirements, so the spacecraft periodically retuned back to the detumbling mode. To drive the spacecraft into the standby mode, the onboard gyros had to be utilized for angular velocity measurements with additional power penalties to the power subsystem. Extensive analysis of the telemetry data lasted for weeks to tune the filter and update the different models onboard such that the filter could provide three-axis attitude and rate information using magnetometer readings only.

The current work uses EgyptSat-1 ADCS design as a test case for the developed filter. In addition to testing the spacecraft during standby mode, the filter is used through the detumbling mode also. First the filter performance is investigated solely, then compared with that of the EKF, and finally its output used to feed the controller to check out the impact of the estimation error and hence the sensor accuracy on the pointing and rate stability of the spacecraft. The satellite has been injected into a near circular Sun-synchronous orbit of a 668-km altitude, 98.085-deg inclination, and 0.001 eccentricity at local mean solar time 22 h 30 min. The first four initials in Table I are given by the launcher from three attitude and rate variances upon separation. The selected variant is the most severe case from the control point of view.

After the separation from the launcher the pitch wheel starts to spin up, providing the spacecraft with a constant momentum in the pitch direction, and the capture process is taken over via three magnetorquers which detumble the satellite to angular velocity less than 0.1 deg/s in 9000 s ($\approx 1.5$ orbits) while the roll and yaw are reconstructed. The satellite starts a pitch maneuver to reconstruct the final attitude and initiates the standby mode to maintain a three-axis pointing accuracy within 5 deg and with a rate less than 0.03 deg/s. The transition between the two phases is according to the condition listed in Table I which incorporates controller gains switching. In addition to these two time windows, another transient 10-min window at the beginning is scoped to investigate the filter transient performance.

The error covariance matrix $\mathbf{P}_0$ is assembled assuming initial errors of 10 deg/s and 175 deg in the angular velocity and attitude, respectively. Also the first three diagonal elements in the process noise covariance matrix $\mathbf{Q}$ are due to torque noises induced by the reaction wheels and/or magnetorquers. As mentioned previously it is assumed to be a zero-mean white noise with a standard deviation $\sigma_\tau = 1.0 \times 10^{-5} N \cdot m$. Dividing by the principle moment of inertia of each axis $\sigma_\omega = \sigma_\tau / I_{ii}$ represents a process noise added to the dynamics in (17).

The other elements of $\mathbf{P}_0$ and $\mathbf{Q}$ are determined by filter tuning. Since the proposed filter is compared with the EKF, the discrete process covariance $\mathbf{Q}_k$ is computed similar to the EKF according to

$$\mathbf{Q}_k = \int_0^{\Delta t} \boldsymbol{\Phi}(\tau) \mathbf{Q} \boldsymbol{\Phi}(\tau)^T dt \tag{38}$$

where

$$\boldsymbol{\Phi} \approx \mathbf{I} + \frac{\partial \mathbf{F}}{\partial \mathbf{x}} \Delta t. \tag{39}$$

The three-axis magnetometer (TAM) senor noise has a standard deviation $\sigma_B = 50$ nT. The induced noise due to measurement differentiation can be approximately calculated as follows:

$$\boldsymbol{\nu}_{\dot{B}_k} = \frac{\boldsymbol{\nu}_{B_{k+1}} - \boldsymbol{\nu}_{B_k}}{\Delta t}. \tag{40}$$

So, it is also a zero-mean white noise with a standard deviation $\sigma_{\dot{B}}^2 = 2\sigma_B^2 / \Delta t^2$.

The magnetic field is modeled using a 10th-order international geomagnetic reference field model. IGRF-2005 is used for this simulation.

To preserve the quaternion normalization constraint in (29), we handled this problem using different methods such as adding a pseudo-measurement or truncating the state vector. For simplicity and reduction of the computational burden, quaternion normalization, namely,

$$\mathbf{q}^*_{k+1/k+1} = \frac{\hat{\mathbf{q}}_{k+1/k+1}}{\|\hat{\mathbf{q}}_{k+1/k+1}\|} \tag{41}$$

is used throughout this work [13].

TABLE I
Simulation Parameters

| | |
|---|---|
| Initial orbital position (km) | $[-1220 \ \ -9665 \ \ 6854]^T$ |
| Initial orbital velocity (km/s) | $[-7.426 \ \ 0.1801 \ \ -1.277]^T$ |
| Initial attitude-Euler angles (deg) | (10 120 30) |
| Initial angular velocity (deg/s) | $[-4 \ \ -4 \ \ -2]^T$ |
| Magnetorquer strength (A.m$^2$) | 10 |
| Pitch wheel bias (N.m.s) | 0.1 |
| Spacecraft dipole $\mathbf{m}$ (A.m$^2$) | $[0.3 \ \ 0.3 \ \ 0.3]^T$ |
| Drag coefficient $C_d$ | 2 |
| Initial state estimate $\mathbf{x}_0$ | $\begin{bmatrix} [0_{1\times3}]^T \\ [0 \ \ 0 \ \ 0 \ \ 1]^T \\ [0_{1\times3}]^T \\ 0 \end{bmatrix}$ |
| Initial error covariance $\mathbf{P}_0$ | $\text{diag}\begin{bmatrix} [0.1745^2 \ \ 0.1745^2 \ \ 0.1745^2]^T \\ [0.04164^2 \ \ 0.04164^2 \ \ 0.04544^2 \ \ 0.9972^2]^T \\ [0.05^2 \ \ 0.05^2 \ \ 0.05^2]^T \\ 0.01^2 \end{bmatrix}$ |
| Process noise covariance $\mathbf{Q}$ | $\text{diag}\begin{bmatrix} [(0.0625\text{e-}5)^2 \ \ (0.0599\text{e-}5)^2 \ \ (0.0704\text{e-}5)^2]^T \\ [0_{1\times4}]^T \\ [(1\text{e-}5)^2 \ \ (1\text{e-}5)^2 \ \ (1\text{e-}5)^2]^T \\ 0.01^2 \end{bmatrix}$ |
| Measurement noise covariance $\mathbf{R}$ | $\text{diag}\begin{bmatrix} [(50\text{e-}9)^2 \ \ (50\text{e-}9)^2 \ \ (50\text{e-}9)^2]^T \\ [(35.35\text{e-}9)^2 \ \ (35.35\text{e-}9)^2 \ \ (35.35\text{e-}9)^2]^T \end{bmatrix}$ |
| UKF special tuning parameters $(\alpha, \beta, \kappa)$ | (1 0 0) |
| Transition from detumbling to standby | $q_{1e}^{br} q_{4e}^{br} \le 0.04 \quad \omega_x^{br} \le 0.0005$ (rad/s)<br>$q_{3e}^{br} q_{4e}^{br} \le 0.04 \quad \omega_z^{br} \le 0.0005$ (rad/s) |
| Detumbling and attitude reconstruction duration | 12000 (s) $\approx$ two orbits |
| Sampling time | 4 (s) |
| Simulation time span | 18000 (s) $\approx$ three orbits |

Figs. 1–4 show the filter performance when operated during the flight scenario simulation. Although the attitude during detumbling is not significantly important and quite difficult to estimate since the focus is only on the angular velocity estimation, the attitude estimation error rapidly decreased from 120 deg to $\pm$20 deg in 10 min, then continued the reduction up to the end of the detumbling phase, and kept the attitude estimation error less than 5 deg in the standby mode. Also, the angular velocity estimation error degraded faster after separation and through detumbling, since the controller task is dedicated to angular velocity suppression, which helped the estimator to converge quickly in rate estimation. Similarly, the estimated spacecraft dipole converged to an error less than $\pm$0.05 A.m$^2$, while the drag coefficient error slowly converged during transition and detumbling since it depends on the attitude which was varying rapidly; once the satellite switched to the standby mode, however, the convergence enhanced significantly.

The second step in testing the filter is to operate against the well-known EKF. The same simulation parameters are used for the EKF. Figs. 5 and 6 show the superiority of the UKF over the EKF since the first converged faster during the transition period, and they kept the same estimation error up to the pitch maneuver starting from 7,000 to 12,000 s. The EKF linearization approximation effect appeared clearly during this hard/fast maneuver. While the UKF kept its convergence trajectory bounded, the EKF fluctuated to higher error values until the end of pitch reconstruction maneuver; then it started to converge again to the designed attitude determination accuracy but is still higher than that resulted from the UKF.

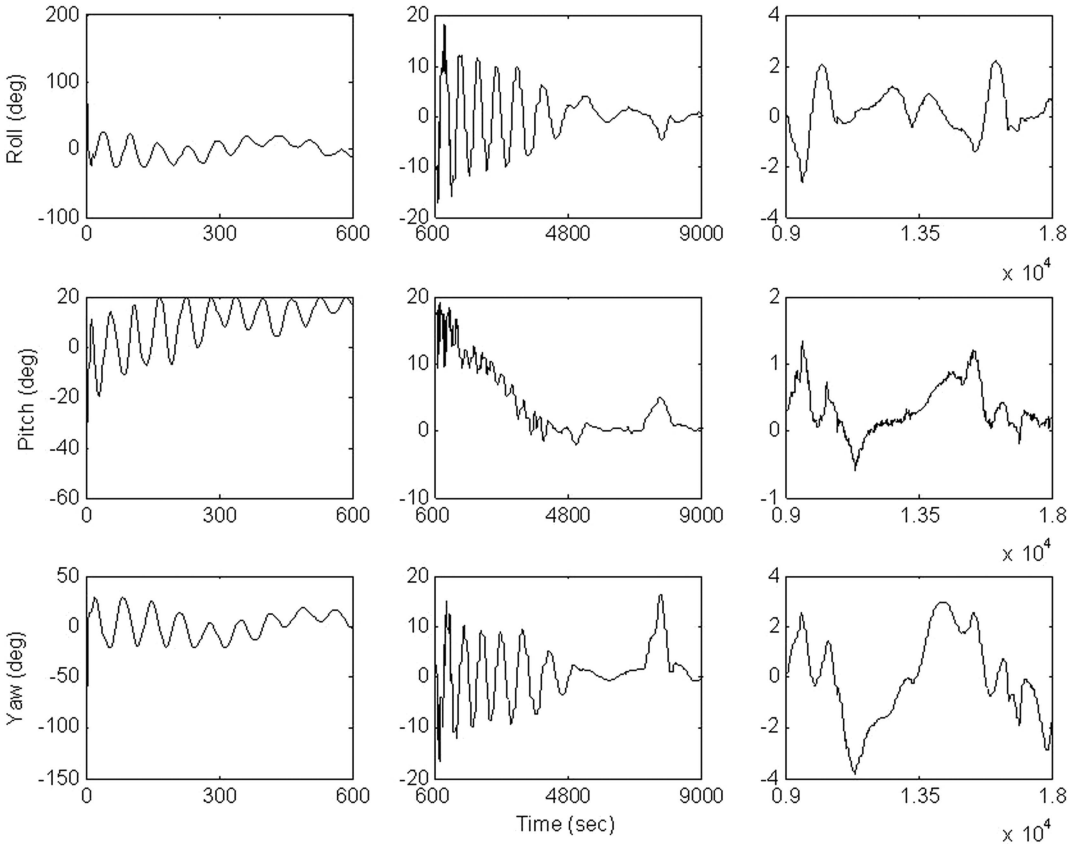


Fig. 1. UKF attitude estimation error (transient-detumbling-standby.

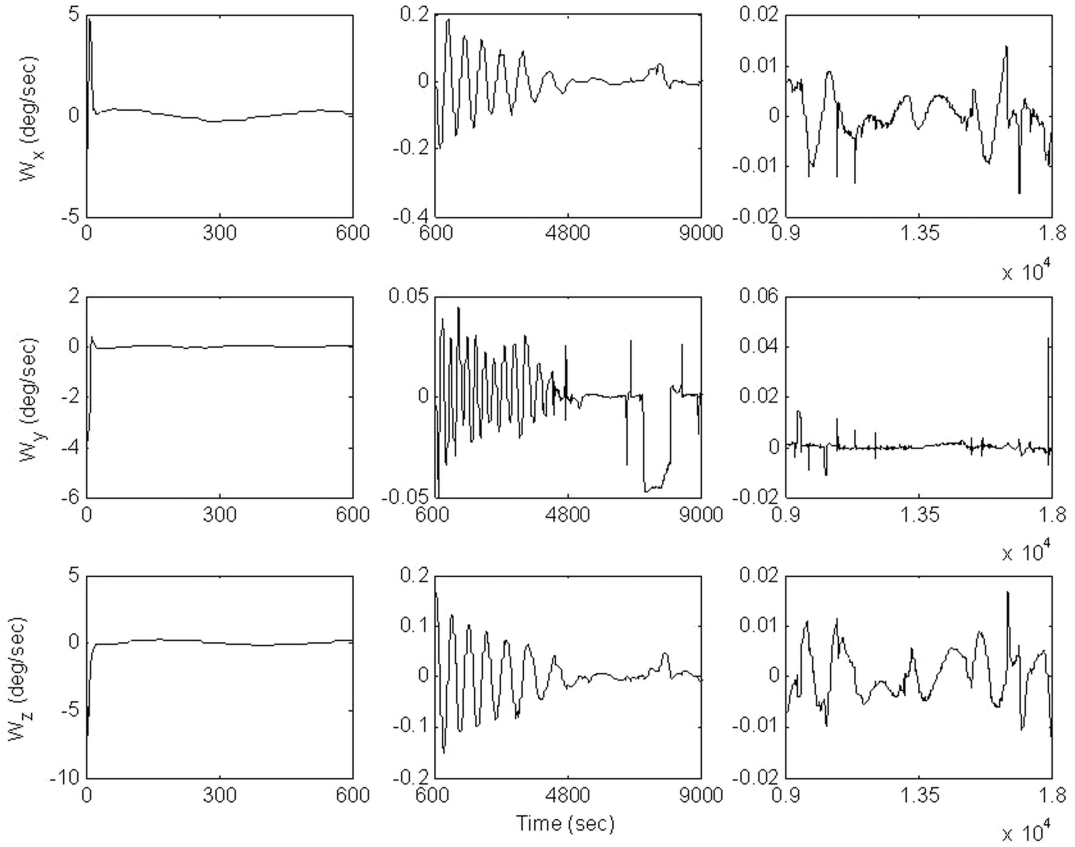


Fig. 2. UKF angular velocity estimation error (transient-detumbling-standby).

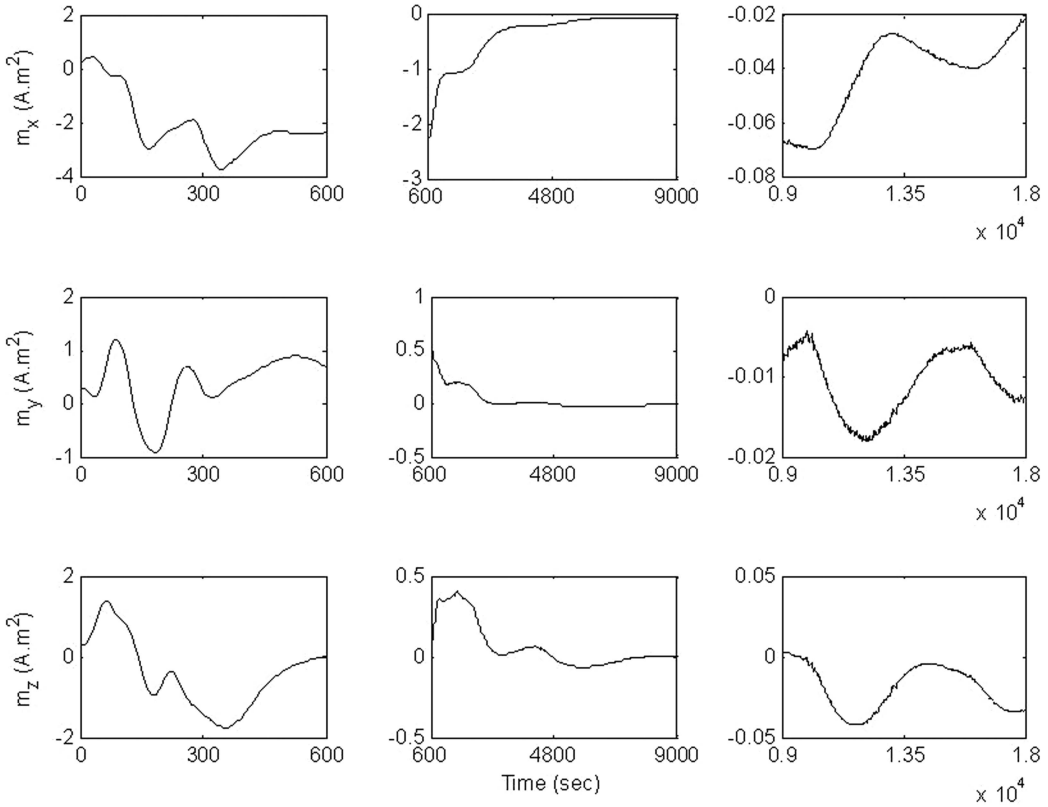


Fig. 3. UKF dipole moment estimation error (transient-detumbling-standby).

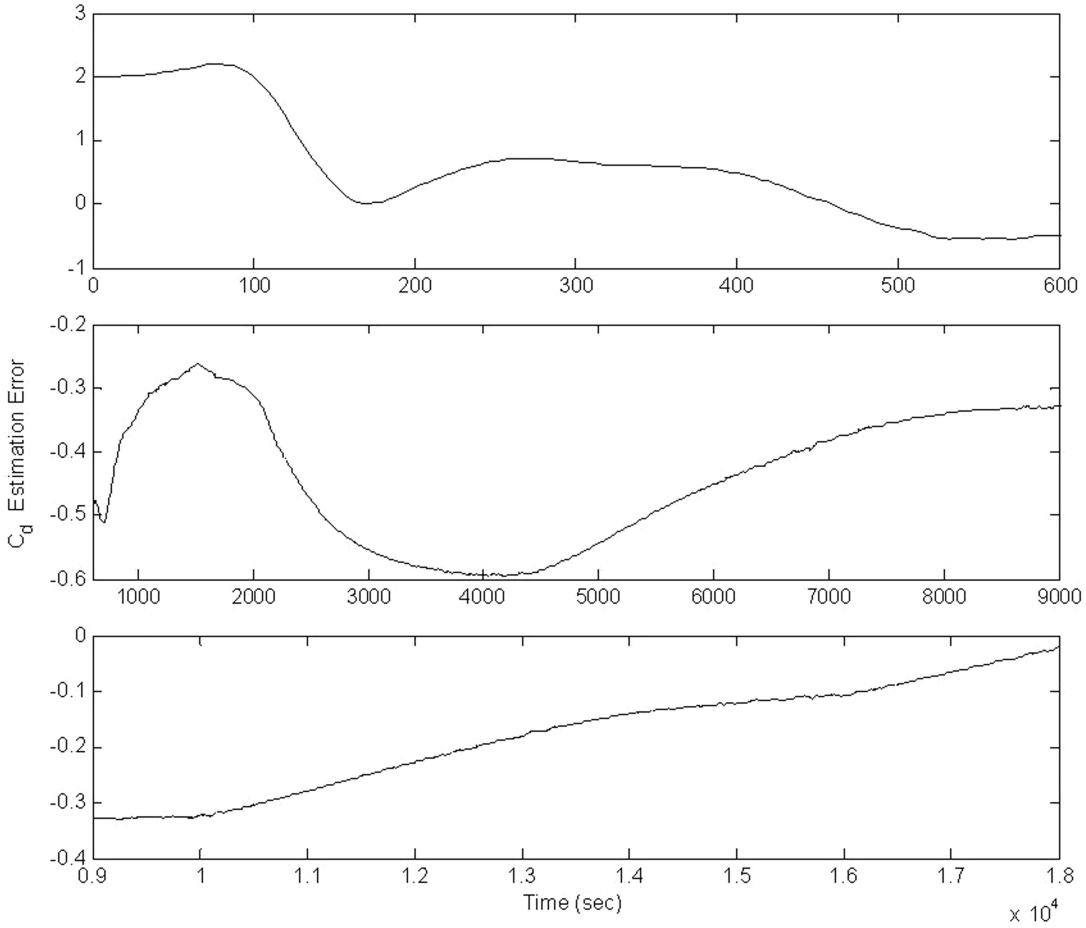


Fig. 4. UKF drag coefficient estimation error (transient-detumbling-standby).

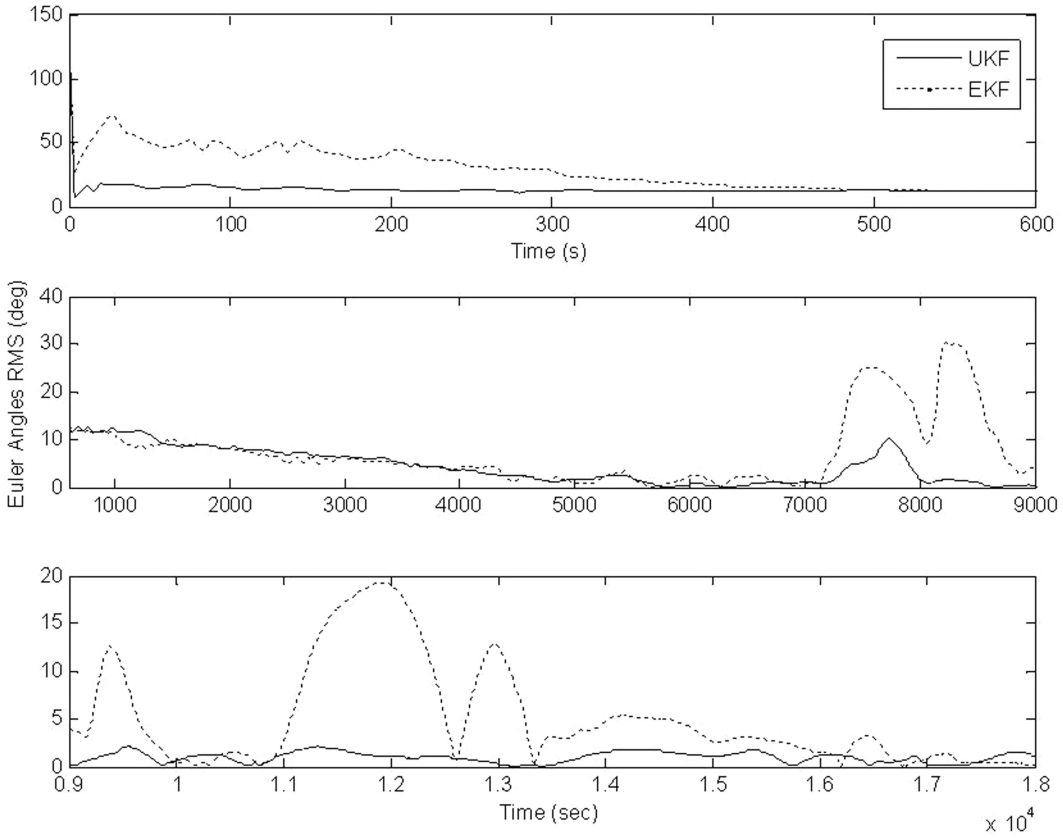


Fig. 5. UKF versus EKF attitude estimation error (transient-detumbling-standby).

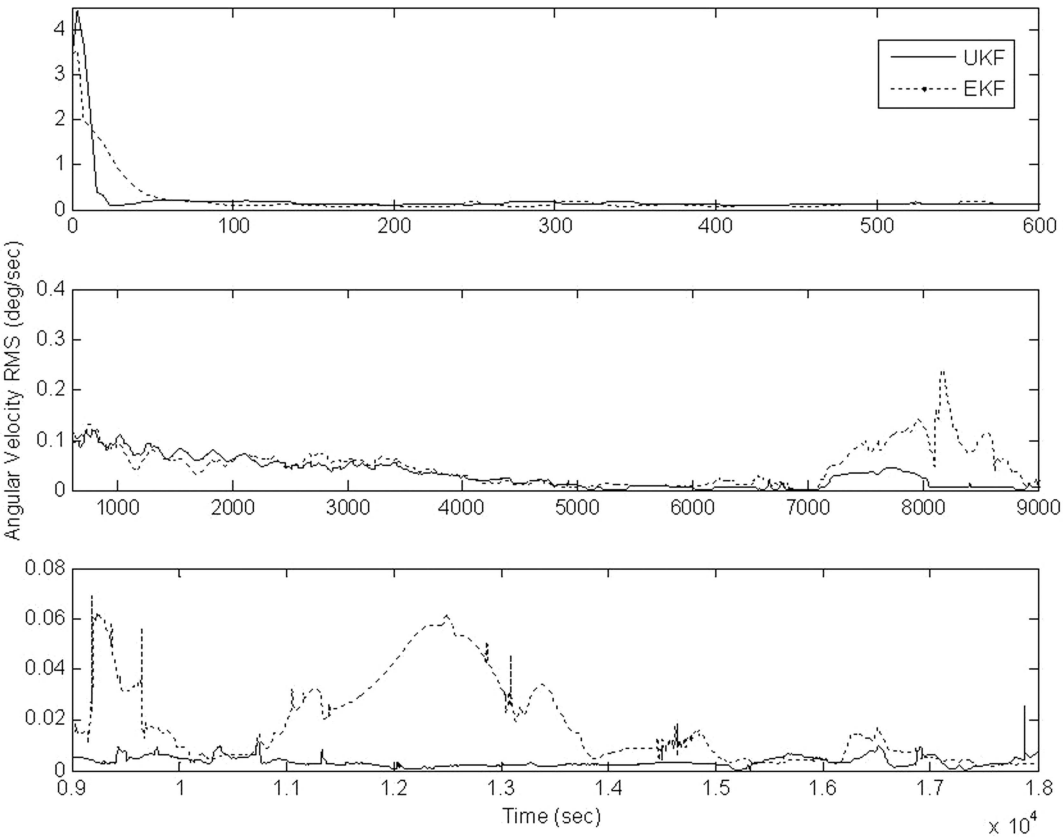


Fig. 6. UKF versus EKF angular velocity estimation error (transient-detumbling-standby).

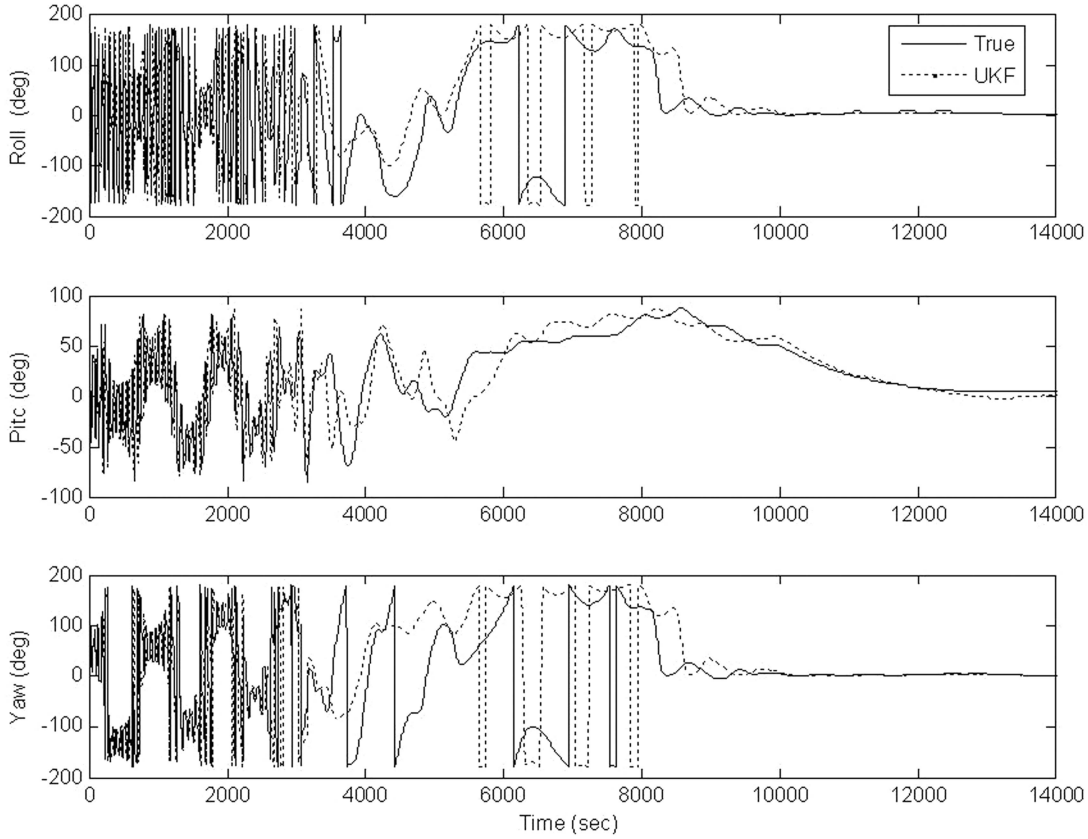


Fig. 7. Attitude history: UKF-based driven controller.

The local observability of the system in (32) and (37) can be applied using the linearized model resulted from the EKF by computing the rank of the following observability matrix:

$$O(\mathbf{H},\mathbf{F},t_0,t_f) = \int_{t_0}^{t_f} \mathbf{\Phi}^T(t)\mathbf{H}^T(t)\mathbf{H}(t)\mathbf{\Phi}(t)dt \quad (42)$$

where

$$\mathbf{H} = \frac{\partial h(\mathbf{x},t)}{\partial \mathbf{x}}. \quad (43)$$

The rank of the observability matrix was found to be 10 when the integral was performed over the sampling time $t_0 \le t \le t_f$ along the simulation time span. Note that although the number of estimated states is 11, the rank of the observability matrix is less by one state: this is due to the quaternion constraint in (29), which is preserved by applying (41) at the end of each estimation cycle.

The following practical step is to use the estimated signals (attitude/rate) to drive the controller in (22).

$$\mathbf{T}_c = -\mathbf{K}_p \hat{q}_{4e}^{br} \hat{\mathbf{q}}_{13e}^{br} - \mathbf{K}_v \hat{\boldsymbol{\omega}}^{br}$$

where $\hat{\mathbf{q}}_e^{br}$ and $\hat{\boldsymbol{\omega}}^{br}$ are calculated using the estimated spacecraft attitude $\hat{\mathbf{q}}$ and angular velocity $\hat{\boldsymbol{\omega}}$.

Figs. 7 and 8 demonstrate the overall performance of the control loop based on the estimated signals' utilization. The true performance is according to the utilization of both magnetometer and gyro measurements for attitude and rate estimation via the EKF algorithm, while the UKF utilized only magnetometer measurements. The objective of these figures is just to demonstrate the capability of the UKF to use one reference sensor to fulfill the mission requirement. The overall performance of the proposed filter successfully fulfilled the mission requirements listed previously. The controller gains have been changed (tuned) to accommodate the new signal characteristics, and consequently the control torque levels have increased as illustrated in Fig. 9 without any change in the magnetorquers strength.

Finally a 100 run Monte-Carlo simulation study was performed to statistically assess the performance of the UKF. The initial attitude (Euler angles) and angular velocity vector were sampled simultaneously from uniform distributions over $[-120,120]$ deg, and $[-5,5]$ deg/s, respectively. Each Monte-Carlo run lasted three orbits (18,000 s), starting from the separation phase up to the detumbling mode and along one orbit in standby mode. The Monte-Carlo means of attitude and angular velocity were computed from the rms along one orbit of standby mode since it is the most dominant mode through the lifetime of the spacecraft. Figs. 10 and 11 summarize the simulation results showing excellent performance of the attitude estimation error, which did not exceed 4 deg and 0.035 deg/s in rate estimation.

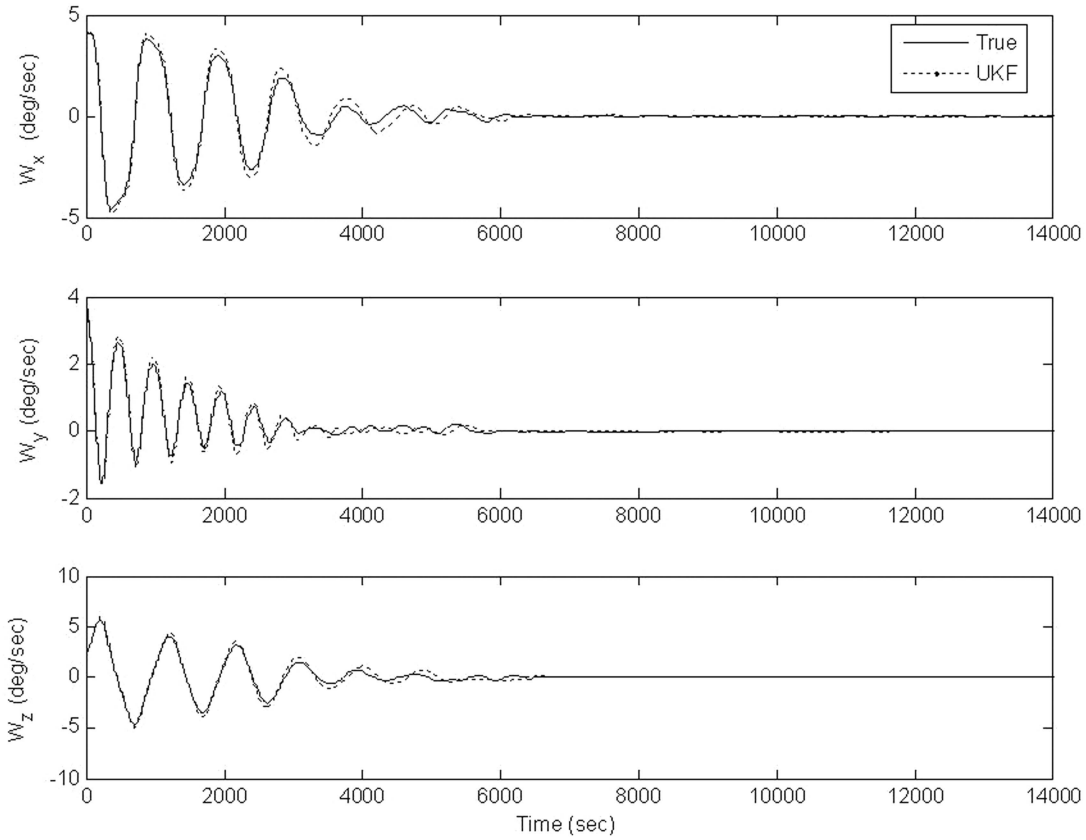


Fig. 8. Angular velocity history: UKF-based driven controller.

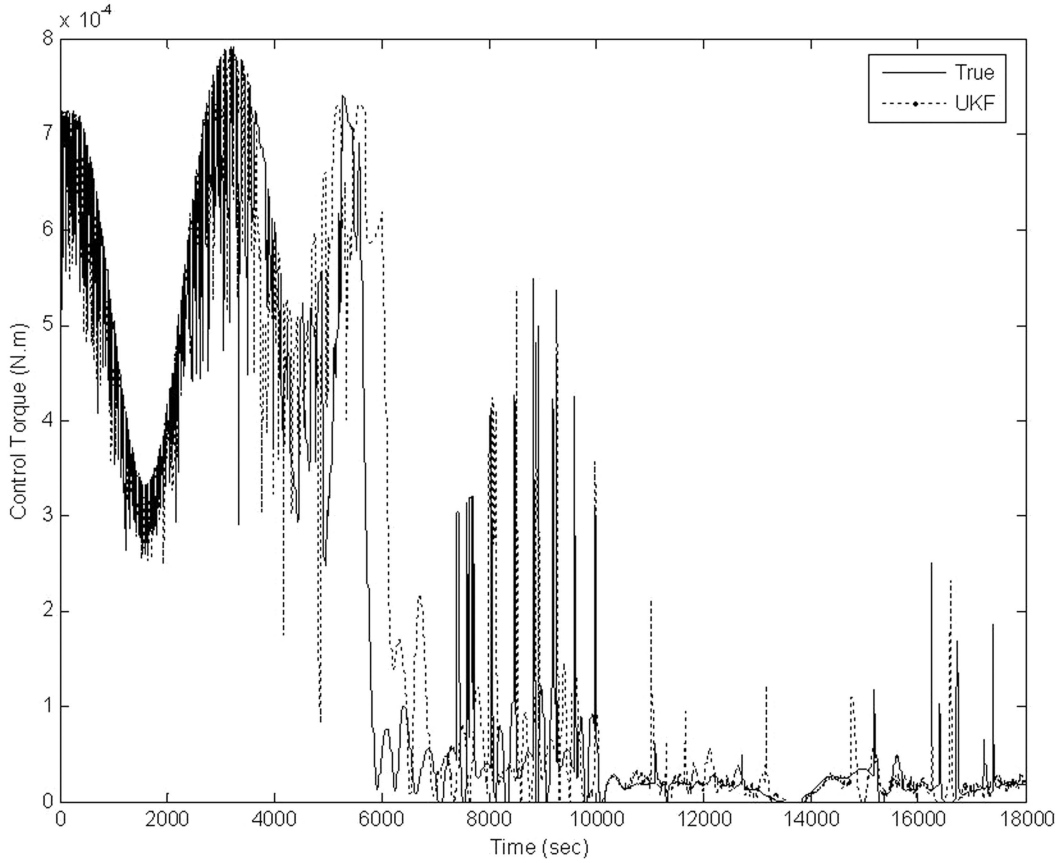


Fig. 9. Control torque history: UKF-based driven controller.

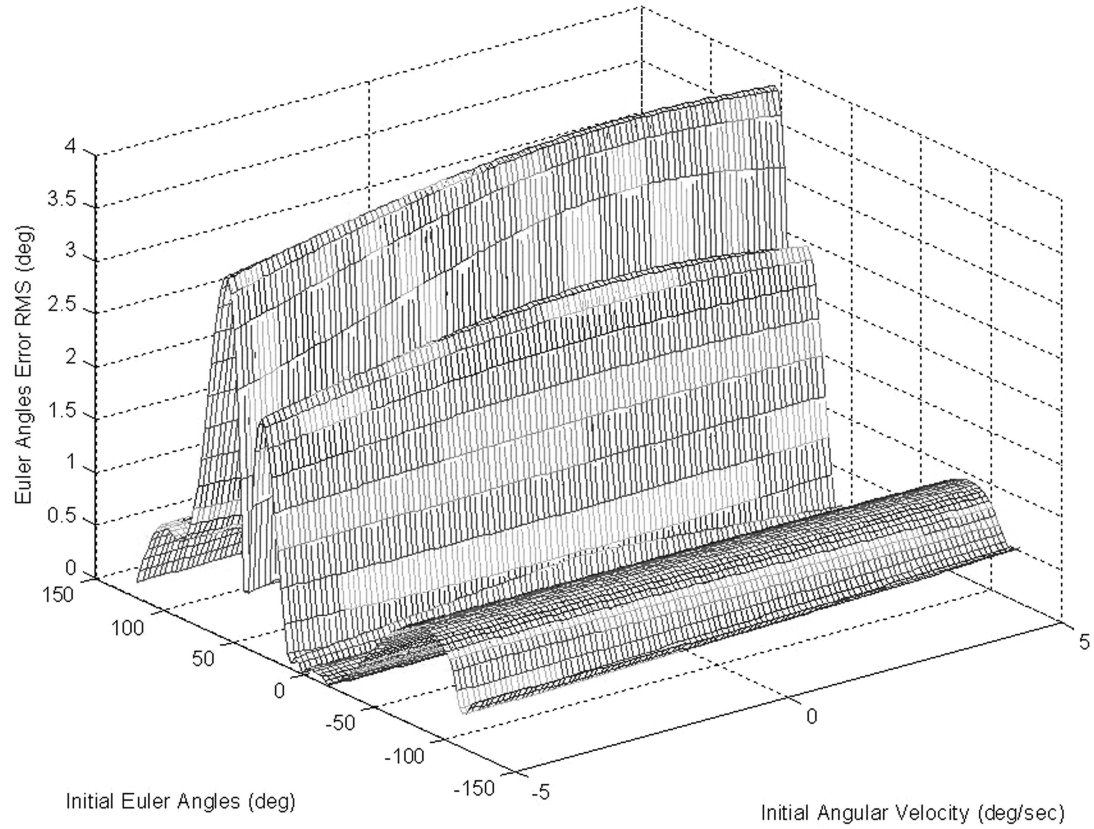


Fig. 10. Attitude error history (Monte-Carlo simulations).

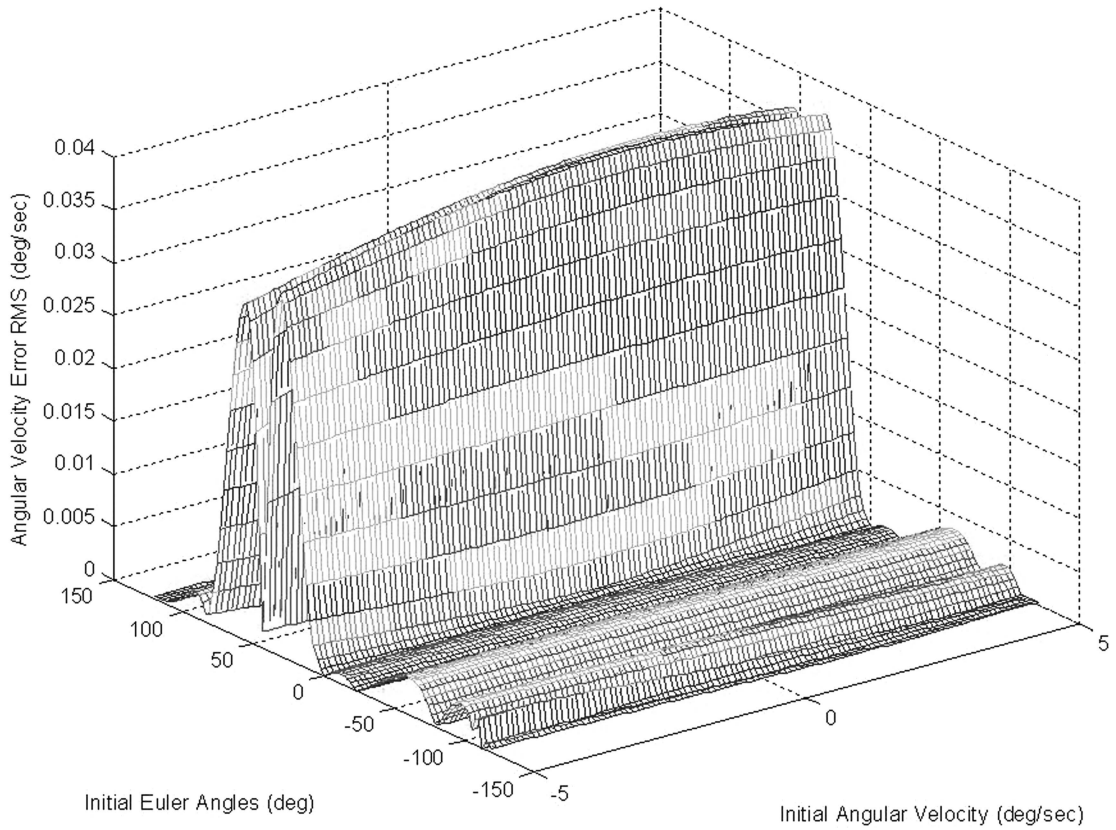


Fig. 11. Angular velocity error history (Monte-Carlo simulations).

## V. CONCLUSION

A spacecraft three-axis attitude and rate estimation algorithm based on magnetometer measurements and their time derivatives has been developed. It has been derived from the family of SPKF and has taken the form of the UKF to handle the addressed problem. In addition to a comparison with the well-known EKF, a Monte-Carlo simulation has been applied to study the performance of the proposed filter with initial attitude and angular velocity sampled from uniform distributions. The filter has been tested to estimate the attitude and rates during satellite detumbling and standby modes of EgyptSat-1, launched in April 2007. The filter has shown the capability of estimating the attitude better than 5 deg and rate on the order of 0.03 deg/s in each axis. The estimated signals have been fed to and utilized by the controller without significant loss in the mission requirements regarding the pointing accuracy and rate stability with bounded increase in the torque levels.

## REFERENCES


[1] Hill, S. and McCusker, T.
Real-time optimal attitude estimation using horizon sensor and magnetometer data.
*Journal of Spacecraft and Rockets*, **35**, 6 (Nov.–Dec. 1998), 778–784.

[2] Azor, R., Bar-Itzhack, I., and Harman, R.
Satellite angular rate estimation from vector measurements.
*Journal of Guidance, Control and Dynamics*, **21**, 3 (May–June 1998), 450–457.

[3] Bar-Itzhack, I.
Classification of algorithms for angular velocity estimation.
*Journal of Guidance, Control and Dynamics*, **24**, 2 (Mar.–Apr. 2001), 214–218.

[4] Challa, M., Natanson, G., and Ottenstein, N.
Magnetometer-only attitude and rates for spinning spacecraft.
In *Proceedings of the AIAA/AAS Astrodynamics Specialists Conference*, Reston, VA, 2000, 311–321.

[5] Crassidis, J. and Markley, F.
Predictive filtering for attitude estimation without rate sensors.
*Journal of Guidance, Control and Dynamics*, **20**, 3 (May–June 1997), 522–527.

[6] Lu, P.
Nonlinear predictive controllers for continuous systems.
*Journal of Guidance, Control and Dynamics*, **17**, 3 (1994), 553–560.

[7] Humphreys, T., Psiaki, M., and Klatt, E.
Magnetometer-based attitude and rate estimation for spacecraft with wire booms.
*Journal of Guidance, Control and Dynamics*, **28**, 4 (July–Aug. 2005), 584–593.

[8] Psiaki, M.
Global magnetometer-based spacecraft attitude and rate estimation.
*Journal of Guidance, Control and Dynamics*, **27**, 2 (Mar.–Apr. 2004), 240–250.

[9] van der Merwe, R. and Wan, E.
Sigma-point Kalman filters for probabilistic inference in dynamic state-space models.
In *Proceedings of The Workshop on Advances in Machine Learning*, Montreal, Canada, June 2003.

[10] van der Merwe, R. and Wan, E.
Sigma-point Kalman filters for nonlinear estimation and sensor-fusion-applications to integrated navigation.
In *Proceedings of AIAA Guidance, Navigation and Control Conference and Exhibit*, Providence, RI, Aug. 2004.

[11] Wan, E. and van der Merwe, R.
The unscented Kalman filter.
In S. Haykin (Ed.), *Kalman Filtering and Neural Networks*, Hoboken, NJ: Wiley, 2001, ch. 7.

[12] LaViola, Jr., J. J.
A comparison of unscented and extended Kalman filtering for quaternion motion.
In *Proceedings of the American Control Conference*, Denver, CO, June 4–6, 2003, 2435–2440.

[13] Bar-Itzhack, I. and Oshman, Y.
Attitude determination from vector observations: Quaternion estimation.
*IEEE Transactions on Aerospace and Electronic Systems*, **AES-21**, 1 (Jan. 1985).

**Mohammad Abdelrahman** was born in 1970. He graduated from Cairo University, Faculty of Engineering, Aerospace Department in 1992, and received from the same department the M.Sc. and Ph.D. degrees in 1998 and 2002, respectively.

During 1995–2000 he worked as a teaching assistant and associate lecturer of automatic control at the Mechatronics Department, Faculty of Engineering October 6th University. From 2000–2007, he worked as a researcher at the National Authority for Remote Sensing and Space Sciences (NARSS), Space Sciences Division. He participated in the Egyptian Space Program and BayernSat project at TÜM, Germany as an ADCS specialist. Also he was a PI and Co-PI for many research projects sponsored by NARSS. Presently he is working as a research professor at the Astrodynamics and Control Lab (ACL), Department of Astronomy, Yonsei University. His current research interests include spacecraft attitude and orbit determination and control, formation flying, hardware in the loop simulation, estimation theory, optimization, nonlinear control, neuro-fuzzy modeling and control, and GPS/INS integration-based systems.

**Sang-Young Park** received the B.S. degree (1986) and the M.S. degree (1988) in astrodynamics from Yonsei University, Seoul, Korea, and the Ph.D. degree in aerospace engineering from Texas A&M University in 1996.

He was a postdoctoral associate supported by the National Academies for the Department of Aeronautics and Astronautics in the Naval Postgraduate School, Montrey, CA, from 1996 to 1998. He was a research assistant professor for the Department of Mechanical Engineering in the same institute from 1998 to 2000. He worked for Final Analysis Inc. in Maryland as a spacecraft systems engineer from 2000 to 2001. He conducted research as a senior spacecraft engineer at NASA Langley Research Center as an employee of Swales from 2001 to 2003. Since 2003, he has been with Yonsei University, where he is professor in the Department of Astronomy. His current reserach interests include satellite orbit determination and control, spacecraft attitude determination and control, satellite formation flying, and trajectory optimization.